Visualizing lowly-populated regions of the free energy landscape of macromolecular complexes by paramagnetic relaxation enhancement†

G. Marius Clore

DOI: 10.1039/b810232e

Many biological macromolecular interactions proceed *via* lowly-populated, highly transient species that arise from rare excursions between the minimum free energy configuration and other local minima of the free energy landscape. Little is known about the structural properties of such lowly-occupied states since they are difficult to trap and hence inaccessible to conventional structural and biophysical techniques. Yet these states play a crucial role in a variety of dynamical processes including molecular recognition and binding, allostery, induced-fit and self-assembly. Here we highlight recent progress in paramagnetic nuclear magnetic resonance to detect, visualize and characterize lowly-populated transient species at equilibrium. The underlying principle involves the application of paramagnetic relaxation enhancement (PRE) in the fast exchange regime. Under these conditions the footprint of the minor species can be observed in the PRE profiles measured for the major species, providing distances between the paramagnetic label and protons of interest are shorter in the minor species than the major one. Ensemble simulated annealing refinement directly against the PRE data permits one to obtain structural data on the minor species. We have used the PRE (a) to detect and characterize the stochastic target search process whereby a sequence-specific transcription factor (the Hox-D9 homeodomain) binds to non-cognate DNA sites as a means of enhancing the rate of specific association *via* intramolecular sliding and intermolecular translocation; (b) to directly visualize the distribution of non-specific transient encounter complexes involved in the formation of stereospecific protein--protein complexes; (c) to detect and visualize ultra-weak self-association of a protein, a process that is relevant to early nucleation events involved in the formation of higher order structures; and (d) to determine the structure of a minor species for a multidomain protein (maltose binding protein) where large interdomain motions are associated with ligand binding, thereby shedding direct light on the fundamental question of allostery *versus* induced fit in this system. The PRE offers unique opportunities to directly probe and explore in structural terms lowly-populated regions of the free energy landscape and promises to yield fundamental new insights into biophysical processes.

Introduction

Conventional crystallography and NMR spectroscopy have yielded a wealth of information on the structures of highly populated static states of biological macromolecules and their complexes. However, little is known about the nature of transient lowly-populated species that cannot be trapped and are therefore effectively invisible to conventional

Laboratory of Chemical Physics, Building 5, National Institute of Diabetes and Digestive and Kidney Diseases, National Institutes of Health, Bethesda, MD 20892-0520, USA. E-mail: mariusc@mail.nih.gov

† This article is part of a *Molecular BioSystems* special issue dedicated to Professor Bruce Alberts on the occasion of his 70th birthday and in recognition of his important contributions to science and education.

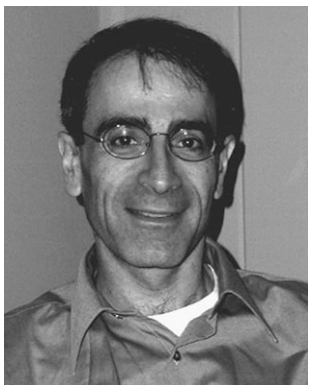

Marius Clore

Marius Clore is chief of the Protein NMR Section at the NIH (1988–present). He received his MD and PhD at University College Hospital Medical School and the MRC National Institute for Medical Research in London, respectively, and was joint head of the Biological NMR Group at the Max Planck Institute for Biochemistry in Germany (1984–1988). His major research interests lie in the application of NMR spectroscopy to study the structure and dynamics of macromolecular complexes.

structural and biophysical methods. Yet many biological interactions proceed *via* the intermediary of such transient states and are also dependent on infrequent but rapid transitions between the global minimum (major configuration) and higher energy local minima within the free energy landscape sampled by macromolecular systems.[1] Indeed, biological interactions are constrained by two opposing requirements of speed and specificity.[2,3] Both kinetic[4–7] and theoretical[8–11] work have suggested, for example, that the rate of formation of stereospecific interactions between macromolecules can be considerably enhanced by a reduction in dimensionality or equivalently the presence of a non-specific attractive potential. For example, the target search process whereby a transcription factor locates its specific target sequence on the DNA among a sea of non-specific sites is thought to be enhanced by processes such as sliding or one-dimensional diffusion along the DNA coupled with hopping from one segment of DNA to another or one molecule of DNA to another.[1] Similarly, the rate of protein–protein complex formation can potentially be enhanced by the formation of non-specific complexes that then relax to the stereospecific complex.[6]

Recent advances in NMR spectroscopy have resulted in the development of two approaches for studying lowly-populated transient species of macromolecules, namely relaxation dispersion spectroscopy[12–15] and paramagnetic relaxation enhancement (PRE).[16–21] The latter is the subject of this *highlight* article. It is important to stress that these lowly-populated states or conformations represent species located in local minima within the free energy landscape and are not to be confused with electronically excited states probed by optical and vibrational spectroscopies (see ref. 22 for a review of many different spectroscopies).

Relaxation dispersion spectroscopy provides quantitative kinetic data characterizing exchange dynamics between major and minor conformational states on the millisecond time scale. In addition, relaxation dispersion experiments yield chemical shift information on the minor species which can be used to obtain low-level, qualitative structural insights into the nature of the minor species. Very recently, experiments that combine relaxation dispersion with weak alignment (through the introduction of liquid crystalline media) have permitted residual dipolar couplings (RDC) and anisotropic chemical shifts to be obtained for minor species, thereby providing highly sensitive bond vector orientation information.[23–25] Relaxation dispersion spectroscopy has seen considerable success in probing lowly-populated species and analyzing their exchange dynamics in diverse systems including protein folding,[14,26,27] enzyme catalysis,[28] protein conformational heterogeneity,[29] and protein–peptide interactions.[30]

The PRE arises from magnetic dipolar interactions between a nucleus such as a proton and the unpaired electrons of a paramagnetic center.[31,32] This effect results in an increase in the relaxation rate of the nuclear magnetization, proportional to the $\langle r^{-6} \rangle$ average distance between the electron and the nucleus of interest. This relationship is analogous to that between interproton distance and the magnitude of the nuclear Overhauser effect (NOE), a phenomenon that lies at the heart of NMR-based macromolecular structure determination.[33,34] In contrast to the NOE, however, where the effect is very small, the PRE effect is very large owing to the large magnetic moment of the unpaired electron and can therefore yield long-range distance information extending up to 35 Å, depending on the paramagnetic group. In the absence of an intrinsic paramagnetic center (such as metalloproteins[35–37]), PRE measurements require the introduction of a paramagnetic group through appropriate conjugation to a specific site.[38] The potential of the PRE for protein structure determination was first demonstrated in the mid 1980s on spin-labeled lysozyme[39] and bovine pancreatic trypsin inhibitor,[40] but was largely neglected until relatively recently with the advent of relatively straightforward biochemical methodology for reliably introducing paramagnetic labels at specific sites.[41–55] In addition, the use of the PRE in rigorous structure determination was thwarted by the fact that extrinsic paramagnetic groups are invariably attached to the macromolecule *via* linkers with multiple rotatable bonds. As a consequence the paramagnetic group is flexible and can sample a wide-range of conformational space, thereby rendering the structural information difficult to interpret. Consequently, any calculation making use of the PRE necessitates treating the paramagnetic center by a multiple conformer representation.[56] To this end the relevant theory and computational tools for direct refinement against PRE data was recently developed and its impact on increasing coordinate accuracy was demonstrated.[56] This work provides the underlying basis for the quantitative interpretation of PRE data arising from minor species.

The PRE is not the only solution spectroscopic method that can provide long-range distance information. Fluorescence resonance energy transfer (FRET) through non-radiative dipole–dipole coupling from the fluorophore, the energy donor, to a second chromophore, the energy acceptor, scales as r^{-6} of the distance r between the two chromophores and can probe separations ranging from 10 to 100 Å.[57] Likewise double nitroxide spin-labeling coupled with pulsed EPR methods such as double electron–electron resonance (DEER), based on the magnitude of the magnetic dipolar coupling of the unpaired nitroxide electrons which scales as r^{-3} of the separation between the nitroxide label, can yield remarkably accurate distances in the 20–60 Å range.[58–61] FRET and EPR methods are not limited by the molecular weight of the system being studied, but suffer from a major drawback in so far that only a single pairwise distance can be measured per sample (*i.e.* each distance requires a new double spin-labeled or double chromophore labeled sample, with the labels in different positions). Thus, although FRET and EPR can yield very specific information they do not afford a practical approach for solving three-dimensional structures of proteins or their complexes. In contrast, while the PRE is limited to the molecular weight range amenable to NMR (currently up to about 150 kDa in very favorable cases), the PRE affords simultaneous probing of a multitude of interactions between a given label and potentially all the observable protons of the system. It is the availability of a very large number of PREs that permits one not only to derive detailed three-dimensional structural information, but also to detect and visualize low population species.

In this *highlight* article we first briefly describe how the PRE is measured and the underlying phenomenon behind the use of the PRE to detect the presence of minor species. We then go on to illustrate the application of the PRE to investigate (a) the dynamic processes involved in the location of a specific cognate DNA binding site by a transcription factor;[16] (b) the formation of non-specific encounter complexes on the pathway to stereospecific protein–protein complex formation;[17] (c) the visualization of ultra-weak protein self-association;[18] and (d) the sampling of lowly populated states involving large scale domain motions in a multidomain protein.[19]

Measuring the PRE

The most useful spin labels for PRE measurements are ones that have an unpaired electron with an isotropic *g*-tensor. Examples include nitroxide spin-labels and EDTA–Mn^{2+}. The isotropic *g*-tensor ensures that the paramagnetic center does not give rise to pseudo-contact shifts and that Curie-spin relaxation is insignificant.[21] The PRE rate, Γ, is given by the difference in relaxation rates measured on a paramagnetic sample and a corresponding diamagnetic control. In general, the most reliable way to make use of the PRE is to measure transverse Γ_2 rates.[21,62] The reason is two-fold. First, the large magnitude of ^{1}H-Γ_2 rates makes the transverse PRE a highly sensitive probe. This is due to the large gyromagnetic ratio of the proton and the fact that the ^{1}H-Γ_2 rate is largely dependent on the spectral density function at zero-frequency. Secondly, the transverse rate is much less susceptible to internal motions and cross-relaxation than the longitudinal PRE rate, ^{1}H-Γ_1.

For proper analysis of PRE data, accurate and reliable ^{1}H-Γ_2 rates are required.[21] Most examples in the literature simply measure peak intensities in the paramagnetic and diamagnetic states but this severely underestimates the true values of the ^{1}H-Γ_2 This is due to the fact that short repetition delays result in recovery levels that are always higher for the paramagnetic sample than the corresponding diamagnetic one owing to the PRE on longitudinal relaxation rates (Γ_1).[62] Accurate ^{1}H-Γ_2 rates, however, can readily be obtained within a reasonable measurement time using a two-time point measurement without requiring any fitting procedures or complicated error estimations.[63]

Underlying phenomenon for the detection of minor species by PRE

The observation of PRE effects for spectroscopically invisible states relies on rapid interconversion between the major and minor species.[16,21] In this type of exchanging system, the observed PREs measured on the resonances of the major species will be modulated by the rate of exchange, k_{ex}, between the major and minor species, and the paramagnetic center–proton distances in the two species. Consider a two-site exchange system comprising a major species (denoted as A), populated at 99%, and a minor species (denoted as B) with an occupancy of only 1%, in which the paramagnetic center–proton distance is 30 Å for the major species and 8 Å for the minor one (Fig. 1). For a 30 kDa system using Mn^{2+} as the paramagnetic label, the ^{1}H-Γ_2 rate will be $\sim$2 s^{-1} for the major species and $\sim$5600 s^{-1} for the minor one. When k_{ex} is slow ($<$50 s^{-1}), the presence of the minor species has no impact on the Γ_2 rate (Γ_2^{obs}) observed on the resonance of the major species; *i.e.* Γ_2^{obs} is equal to the Γ_2 rate for the major species, Γ_2^A. As k_{ex} increases, Γ_2^{obs} increases, and in the fast exchange limit, defined as $k_{ex} \gg (\Gamma_2^A - \Gamma_2^B)$, is given by the weighted population average of the two species: $\Gamma_2^{obs} = p\Gamma_2^A - (1-p)\Gamma_2^B$, where p is the fractional population of the major species. In this example, Γ_2^{obs} in the fast

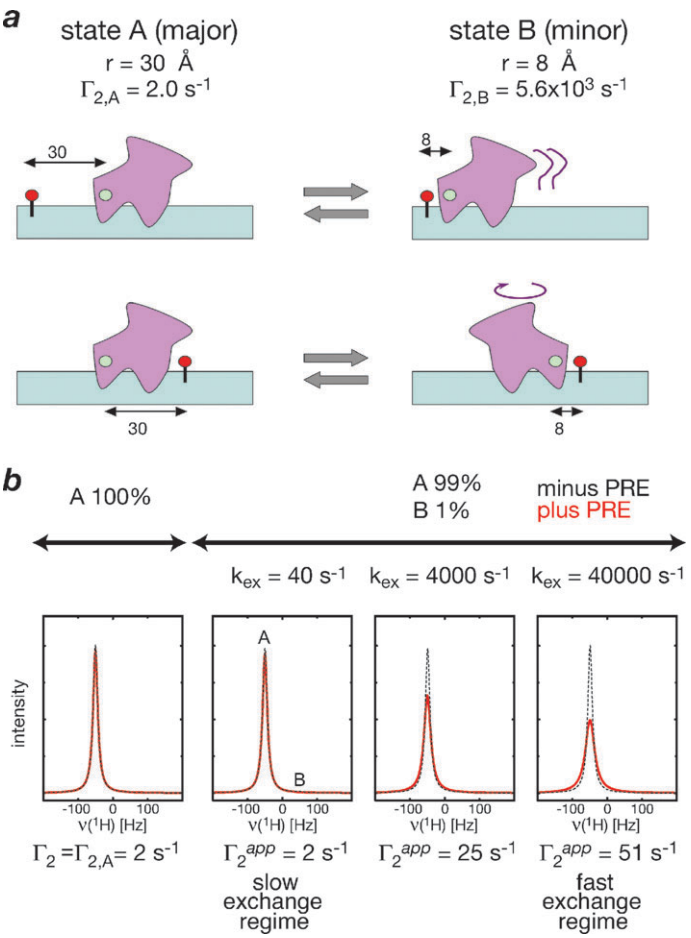

Fig. 1 Intermolecular PRE in an exchanging system. (a) Diagrammatic depiction of a two site-exchange process involving major (99%) and minor (1%) species with paramagnetic–^{1}H distances of 30 and 8 Å, respectively. (b) Effect of increasing exchange rate on NMR line-shape with (red) and without (black) PRE. In the slow exchange regime the PRE is insensitive to the presence of the minor state; in the fast exchange regime, however, the PRE is sensitive to the presence of a minor species and can be used to reveal its footprint. Adapted from ref. 16.

exchange regime is ~ 30 times faster than Γ_2^A. Thus, in the fast exchange regime, providing the corresponding paramagnetic center–proton distance is shorter in the minor species than the major one, Γ_2^{obs} will include a contribution from the minor species, allowing one to both infer the presence of the minor species and derive structural information on it.[16–19] The latter is obtained not from a single PRE observed on a single proton, but from multiple PREs observed on the large number protons in the system. This is crucial since the footprint of the minor species can only be ascertained by discrepancies between the PREs that are not consistent with a single configuration.

Target location in specific protein–DNA interactions

A long-standing question in protein–DNA recognition pertains to the search process whereby a transcription factor locates its specific cognate site among a sea of non-specific sites.[2] Kinetic and theoretical considerations have provided strong evidence that non-specific binding can significantly enhance the rate of specific recognition by two complementary mechanisms:[2–5] (a) intramolecular translocation or sliding along the DNA that effectively reduces the dimensionality of the search procedure from three dimensions to one dimension; and (b) intermolecular translocation or hopping from one DNA molecule to another or from one DNA segment to another *via* looping. We investigated these pheno mena using the HoxD9 homeodomain–DNA complex as a model system.[16] Homeodomains are found in many eukaryotic transcription factors, possess well-characterized sequence-specific DNA-binding activity,[63] and have been extensively studied by both crystallography[64] and NMR spectroscopy.[65]

At 100 mM NaCl the equilibrium dissociation constant for the specific HoxD9–DNA complex, determined by fluorescence anisotropy, is 1.5 nM[16] and the dissociation rate constant determined by gel shift assays at very low (nM) concentrations of the DNA is $\ll 0.01\ s^{-1}$.[66,67] However, $^{15}N_z$-exchange spectroscopy indicates that the overall exchange rate for direct intermolecular transfer between DNA specific sites located on two DNA duplexes differing by only a single base pair mutation just outside the central specific binding site is substantial, ranging from $\sim 7\ s^{-1}$ at 20 mM NaCl (slow exchange regime) to $600\ s^{-1}$ at 160 mM NaCl (fast exchange regime).[16,68] The exchange process monitored by $^{15}N_z$ exchange spectroscopy is directly proportional to the concentration of free DNA, and hence does not involve dissociation of DNA-bound protein into free solution followed by reassociation, but rather proceeds *via* direct transfer following collision of free DNA with DNA-bound protein without ever going through the intermediary of free protein.[68] This process dramatically accelerates the rate of target recognition resulting in translocation rates that are over 3–4 orders of magnitude faster than the dissociation rate constant, and reconciles the highly dynamic behavior of protein DNA complexes observed *in vivo* using microscopy combined with fluorescence recovery after photobleaching (FRAP)[69] with the long half-lives of specific protein–DNA complexes measured by traditional biochemical analysis *in vitro*.[66,67]

For PRE experiments, we examined a complex of U-[$^{15}N/^2H$]-labeled HoxD9 with a 24-bp DNA duplex at natural isotopic abundance in which the specific target site was located in the middle of the DNA, and four different dT sites, labeled one at a time, were conjugated to an EDTA–Mn^{2+} paramagnetic probe (Fig. 2a and b).[16] The latter is located in the major groove of the DNA. At low salt (20 mM NaCl), in the slow exchange regime, the intermolecular PRE data are fully consistent with the known structure of the complexes with a PRE Q-factor of 0.26 (Fig. 2c). Large magnitude intermolecular PREs are only observed for those regions in relatively close proximity to the dT–EDTA–Mn^{2+} group (Fig. 2e). As the salt concentration is raised (to 100 and 160 mM NaCl), however, the intermolecular PRE data are completely inconsistent with the structure (Fig. 2f); the correlation between observed and calculated Γ_2 rates is very poor with a PRE Q-factor of 0.66 (Fig. 2d). Thus, residues located on the opposite face of HoxD9 relative to the location of the dT–EDTA–Mn^{2+} groups exhibit large intermolecular PREs (Fig. 2f). These PRE profiles cannot be accounted for by any single location of HoxD9 on the DNA. Further, the change in PRE profile with increasing salt concentration is not due to any changes in structure since the ^1H–^{15}N correlation spectrum of the HoxD9–DNA complex remains unaltered and RDCs at low and high salt are highly correlated ($r = 0.99$). Thus, the intermolecular PRE data at high salt reflect the footprint of minor species that exchange rapidly with the specific complex. The HoxD9 homeodomain in these minor states is bound stochastically to various sites along the DNA and can therefore come into close proximity to the paramagnetic labels (Fig. 2b). The population of the minor species is estimated to be less than 1%, based on the observed equilibrium dissociation constants at 100 mM NaCl of 1.5 and 270 nM for specific and non-specific DNA binding, respectively.[16]

The PRE profile also provides qualitative structural information on the minor species since the regions that exhibit large PREs exclusively involve residues close to or at the DNA binding interface and can therefore readily come into close proximity with the paramagnetic labels (Fig. 2f).[16] Regions with small PREs, such as the C-terminal half of helix 1, on the other hand, are located distant from the DNA interface. One can therefore conclude that the DNA binding mode adopted during the target search process is similar to that in the specific complex, and that the population of any alternate configurations, should these
exist, are below the limits of detection. That the non-specific binding mode of HoxD9 is virtually identical to that of the specific complex was later confirmed in a combined PRE and RDC study of a dynamic ensemble of non-specific HoxD9–DNA interactions.[70]

Two processes can potentially contribute to the PRE profiles observed on the specific HoxD9–DNA complex at high salt, namely intramolecular sliding and intermolecular translocation. To ascertain the relative contributions of these two processes, we performed two experiments with HoxD9 in the presence of equal concentrations of two DNA duplexes, one with and the other without the specific DNA recognition site (Fig. 3).[16] In the first sample only the non-specific

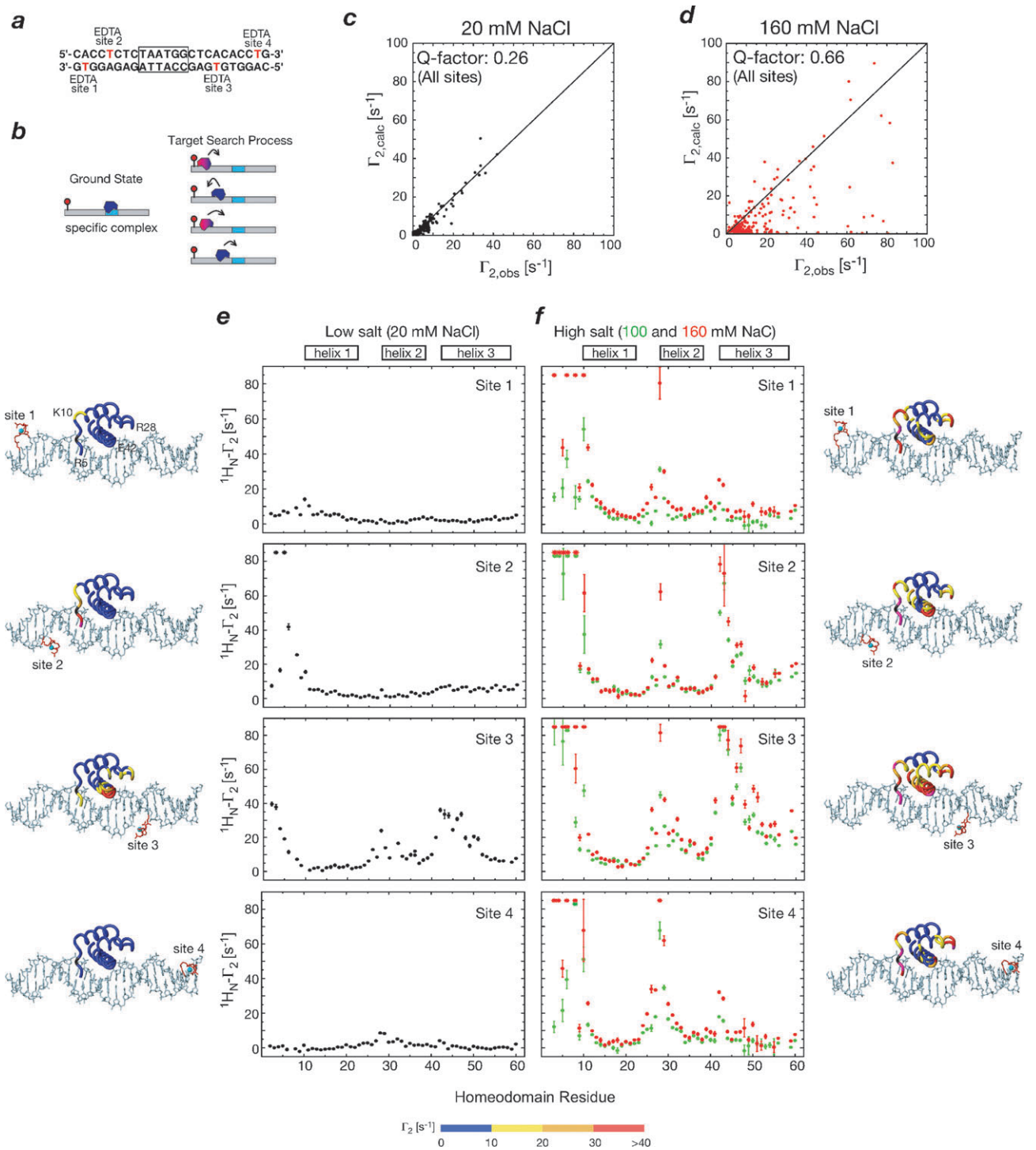

Fig. 2 Intermolecular PREs observed for the HoxD9–DNA complex in the slow (20 mM NaCl) and fast (160 mM NaCl) exchange regimes. (a) DNA duplex containing the HoxD9 specific binding site (boxed) and showing the location of the 4 sites used to introduce dT–EDTA–Mn^{2+} (one at a time). (b) Schematic illustration of the ground state specific complex and the target search process. (c) and (d) Correlation between observed and calculated PREs for all 4 sites at low (20 mM NaCl) and high (160 mM NaCl) salt, respectively. (e) and (f) PRE profiles at low (20 mM NaCl) and high (100 and 160 mM NaCl) salt, respectively. On either side of the PRE profiles, the PRE data are mapped on the structural model of the HoxD9–DNA complex, with the color scale depicting Γ_2 rates. Adapted from ref. 16.

DNA duplex bears the paramagnetic label, while in the second sample the converse scheme is employed with only the specific DNA duplex bearing the paramagnetic label (Fig. 3a). Thus, in the case of sample 1 intermolecular PREs can only be observed if rapid intermolecular translocation between the specific and non-specific DNA duplexes occurs. For sample 2, however, intermolecular PREs can arise from both intramolecular sliding and intermolecular translocation. The overall PRE profiles for the two samples are very similar, indicating that intermolecular translocation is a major

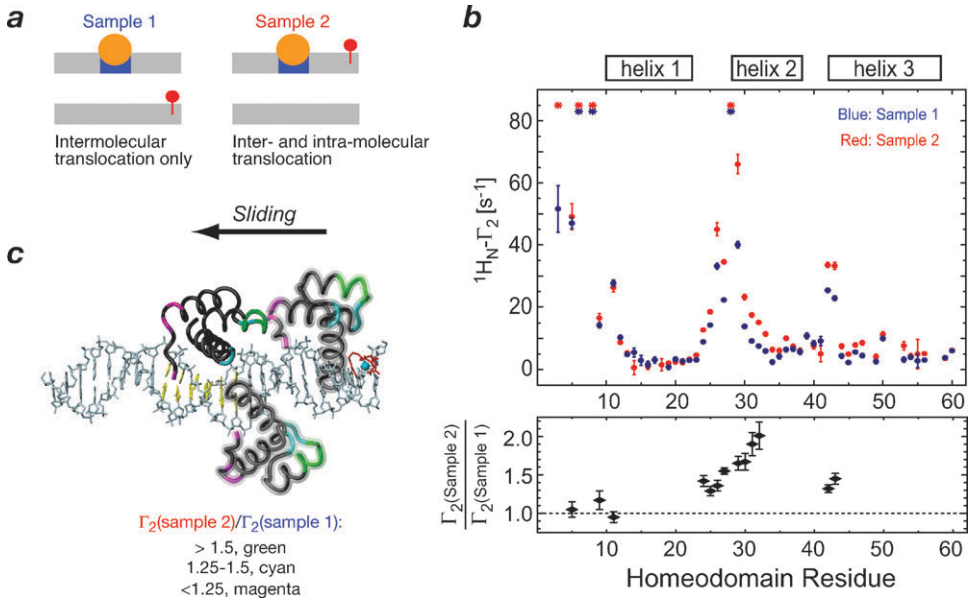

Fig. 3 Intramolecular sliding and direct intermolecular translocation in the HoxD9–DNA system. (a) PRE data were collected on HoxD9 in the presence of an equal mixture of two DNA duplexes, one with and the other without the specific site (indicated in blue). In sample 1, the non-specific DNA bears the paramagnetic center and PREs only arise from intermolecular translocation; in sample 2, the specific DNA has the paramagnetic center and PREs can arise from both intramolecular sliding and intermolecular translocation. (b) Observed PRE profiles. (c) Schematic representation of sliding along the DNA with HoxD9 color coded according to the Γ_2(sample 2)/Γ_2(sample 1) ratio. Adapted from ref. 16.

contributor (Fig. 3b). However, the PRE values for residues 2–44 and 41–42 are 30–100% larger for the second sample than the first, whereas the PREs for the N-terminal arm are identical in the two samples (Fig. 3b). The larger PRE values for specific regions of HoxD9 in sample 2 are directly attributable to intramolecular sliding which gives rise to bias owing to the fact that the orientation of HoxD9 bound to the specific site is favored as the protein slides along the DNA (Fig. 3c). Thus, as the protein slides away from the specific site, residues 23–33 and 41–42 can readily come into close contact with the paramagnetic label, whereas the N-terminal tail, however, can only approach the paramagnetic center following an intermolecular translocation event resulting in a 180° change in binding orientation of the protein on the DNA duplex.

Transient encounter complexes in protein–protein recognition

Kinetic data on a number of protein–protein associations have provided evidence for the initial formation of a pre-equilibrium encounter complex that subsequently relaxes to the final stereospecific complex. Further, site-directed mutagenesis[6–8] and Brownian dynamics[9–11] simulations have suggested that the rate of association can be modulated by perturbations in charge distribution outside the direct interaction surfaces. This suggests that non-specific encounter complexes may also play a role in protein–protein recognition by facilitating the formation of the stereospecific complex.

We set out to detect encounter complexes in protein–protein association using intermolecular PRE measurements.[17] The system we chose to study was the relatively weak (K_{diss} ~ 1 mM) complex between the N-terminal domain of enzyme I (EIN) and the histidine phosphocarrier protein (HPr) of the bacterial phosphotransferase system.[71] Exchange between free and bound states of the proteins is fast on the chemical shift time scale.[72] The structures of EIN and HPr have been solved by both crystallography[73,74] and NMR spectroscopy,[75–77] and the structure of the EIN–HPr complex has been solved by NMR spectroscopy on the basis of extensive NOE and RDC data.[71] This complex catalyzes the reversible transfer of a phosphoryl group from the Nε2 atom of His189 of EIN to the Nδ1 atom of His15 of HPr. The NMR structure of the complex is fully consistent with the formation of a pentacoordinate phosphoryl transition state intermediate without requiring any significant structural perturbation.[71] Paramagnetic labels in the form of EDTA–Mn^{2+} were conjugated (one at a time) to three engineered surface cysteine residues on HPr (E5C, E25C and E32C) located outside the binding surface with EIN (Fig. 4).[17]

The intramolecular ^1H_N-Γ_2 rates for HPr within the EIN–HPr complex are fully consistent with the structure of HPr, with a PRE Q-factor for all three sites combined of only 0.18 (Fig. 4a). A comparison of the intermolecular PRE profile measured on EIN, however, shows that while features attributable to the stereospecific complex are clearly present, other features cannot be accounted for by either the stereospecific complex or any single alternative configuration, and reflect the presence of an ensemble of alternative binding modes involving non-specific encounter complexes (Fig. 4b).[17] As a result the overall PRE Q-factor calculated using the stereospecific complex is high with a value of 0.61 and the correlation between observed and calculated Γ_2 rates is poor (Fig. 4c).

To derive a semi-quantitative structural description of the encounter complex ensemble from the intermolecular PRE data we made use of direct rigid body simulated annealing refinement[17,78] against the

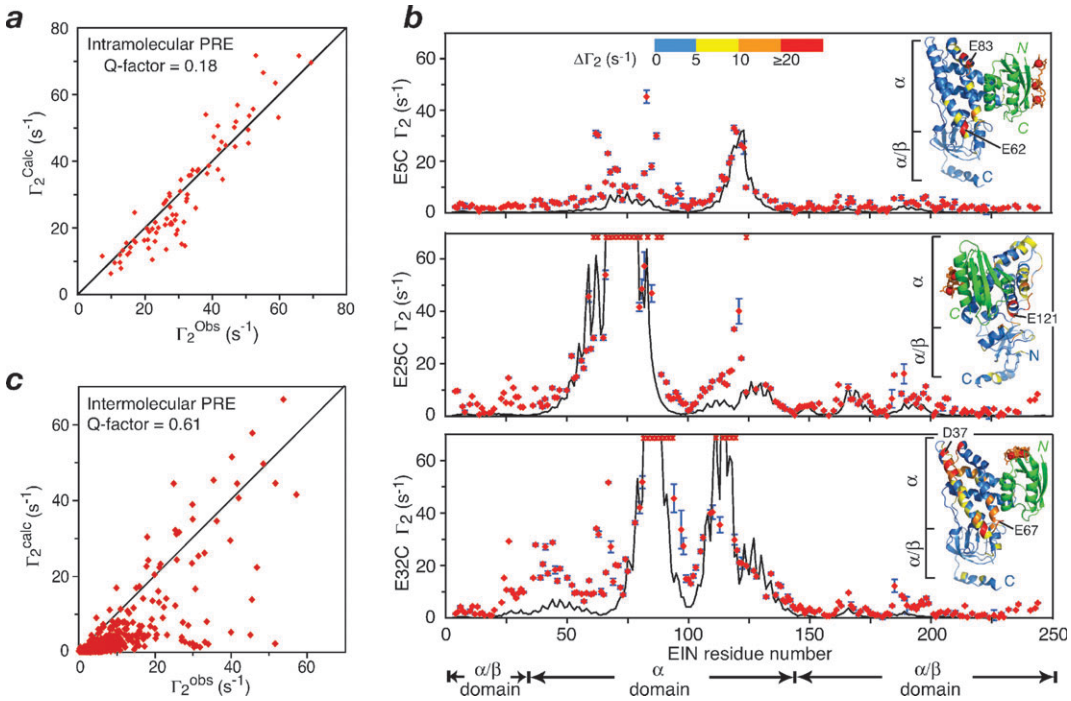

Fig. 4 Intermolecular PREs for the EIN–HPr complex. EDTA–Mn^{2+} was conjugated to an engineered surface cysteine at 3 sites (E5C, E25C and E32C). (a) Correlation between observed and calculated intramolecular Γ_2 rates for HPr. (b) Intermolecular PRE profiles observed for the 3 sites, with experimental Γ_2 rates denoted by the red circles, and the theoretical Γ_2 rates calculated from the structure of the stereospecific complex by the black line. (c) Correlation between observed and calculated intermolecular Γ_2 rates measured on EIN and arising from paramagnetically labeled HPr. Adapted from ref. 17.

PRE data. The representation employed comprised the stereospecific complex (whose structure is fixed) with population p in rapid exchange with an ensemble of encounter complexes comprising N states with population $(1 - p)$ (Fig. 5a). Complete cross-validation indicated that the optimal ensemble size was 10–20 (Fig. 5b) at a population of ~10% (Fig. 5c). The resulting overall Q-factor is 0.21 (Fig. 5d).[17]

The distribution of non-specific encounter complexes is best visualized as an atomic probability map[79] (Fig. 5e). Two features stand out. First, there is a qualitative correlation between the encounter complex distribution and the electrostatic surface potential, with the positively charged face of HPr populating regions of EIN with high negative electrostatic potentials. Second, the region occupied by the stereospecific complex is minimally populated by non-specific encounter complexes, suggesting that once HPr reaches this region formation of the stereospecific complex occurs with high probability.

The relevance of weak non-specific electrostatic interactions in the formation of non-specific encounter complexes can be probed by examining the salt dependence of the intermolecular PREs.[80] The magnitude of the intermolecular PREs that can be directly attributed to the stereospecific complex shows only a small dependence on salt concentration and can be accounted for by the dependence of the overall equilibrium dissociation constant on salt concentration. The magnitude of the PREs originating from the ensemble of non-specific encounter complexes, however, shows a much larger salt dependence. Thus, the population of non-specific encounter complexes is modulated to a significantly greater degree by ionic strength than the stereospecific complex. This finding is fully consistent with Debye–Hückel theory. Interfacial packing is on average less compact in the non-specific encounter complexes than in the stereospecific complex.[17] Hence the average intermolecular distance between oppositely charged residues is significantly longer in the non-specific complexes than the stereospecific one, thereby permitting more effective screening of intermolecular electrostatic interactions by ions in solution.[80]

The picture that emerges from this study is one in which weak, highly transient non-specific encounter complexes are initially formed by weak long-range electrostatic interactions, supplemented by short range van der Waals interactions. The life-times of the non-specific encounter complexes are sufficiently long to permit a two-dimensional search on the surface of the proteins until the region of the specific interaction surfaces is reached and the complex falls down a narrow energy funnel.[81–83] The stereospecific complex is located at the minimum of this free energy funnel and is characterized by an array of complementary van der Waals and electrostatic interactions.

The findings on the EIN–HPr complex are quite general and direct detection of non-specific encounter complexes by PRE has been observed for several other weak protein–protein complexes, including two other complexes involving HPr and the proteins $IIA^{mannitol}$ and $IIA^{mannose}$,[17] and redox complexes of cytochrome c with cytochrome c peroxidase and adrenodoxin.[20,84]

Ultra-weak protein self association

Ultra-weak macromolecular self-association (K_{diss} > 10 mM) is exceptionally

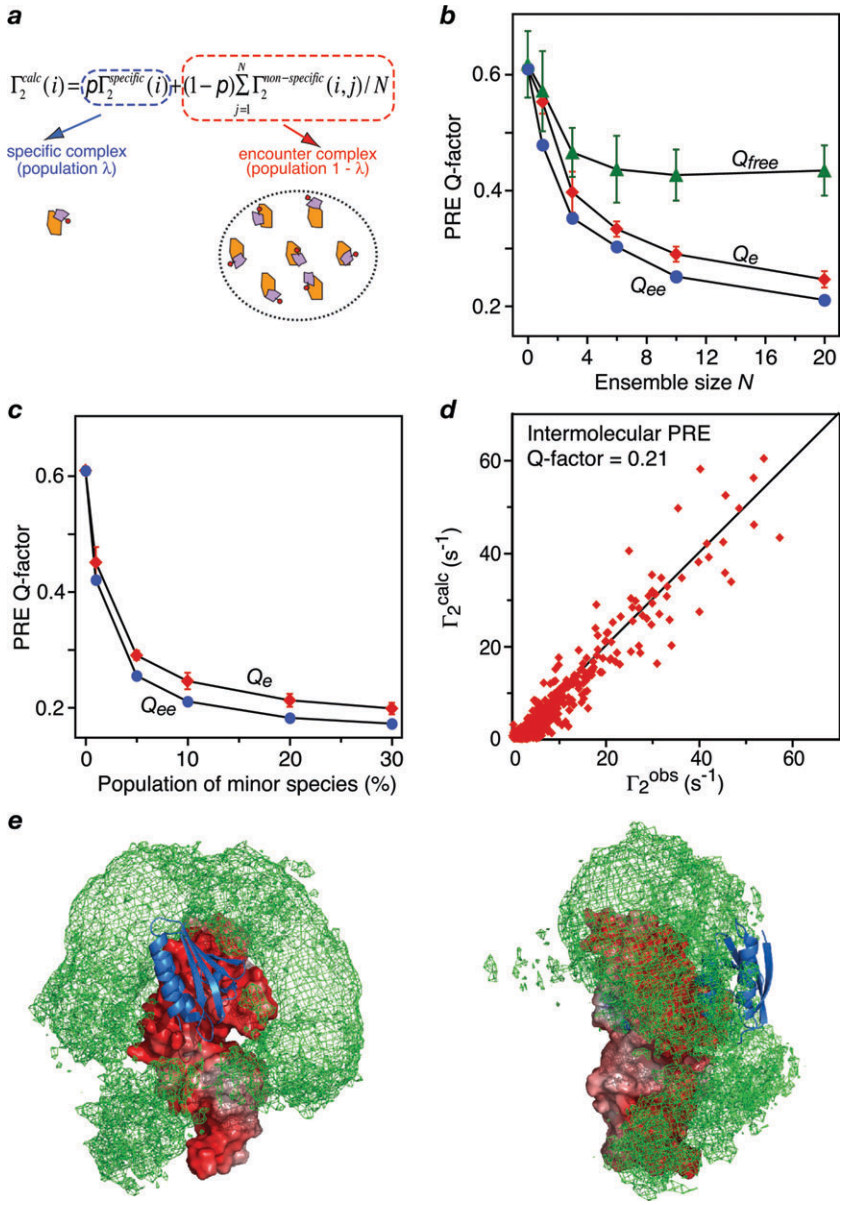

Fig. 5 Ensemble refinement of intermolecular PRE data for the EIN–HPr complex. (a) The observed Γ_2 rates in the fast exchange regime are a weighted average of the Γ_2 rates for the specific complex and an encounter complex ensemble comprising N species. (b) Dependence of working (Q_e and Q_{ee}) and complete cross-validated (Q_{free}) Q-factors on ensemble size N. (Q_e is the average Q-factor $<Q>$ for all 100 calculated ensembles, and Q_{ee} is the ensemble of ensembles average Q-factor). (c) Dependence of working Q factors on population of the encounter complex ensemble. (d) Correlation between observed and calculated Γ_2 rates obtained with a population of 10% for the encounter complex species represented by an ensemble of size $N = 20$. (e) Two views of a reweighted atomic probability density map[79] illustrating the distribution of HPr molecules on the surface of EIN that make up the ensemble of encounter complexes. The encounter complex probability map (green mesh plotted at a threshold of 20% maximum) is calculated from 100 independent calculations of ensemble size $N = 20$ at a population of 10%; the molecular surface of EIN is color coded by electrostatic potential ($\pm 8kT$); and the location of HPr in the stereospecific complex is shown as a blue ribbon. Adapted from ref. 17.

difficult to detect by conventional biophysical techniques owing to the very low population of the self-associated species, yet such weak intermolecular interactions coupled with nucleation events play a critical role in driving spontaneous self-assembly to form higher-order architectures.[85–87]

We chose to investigate ultra-weak self-association of HPr using the PRE.[19] Sedimentation velocity experiments yield excellent fits to a single species with a molecular mass fully consistent with monomeric HPr (~9 kDa) and provide an upper limit of only 1–2% for any higher order soluble species. Intermolecular PRE measurements were carried out using a 1 : 1 mixture of U-[^{15}N]-labeled HPr with HPr paramagnetically labeled with EDTA–Mn^{2+} at three different sites individually (E5C, E25C and E32C). Large intermolecular PRE effects, above the background observed with hydroxylamine–EDTA–Mn^{2+} as a control, were observed for two of the three paramagnetically labeled sites, E5C and E32C, indicative of very weak self-association (Fig. 6a). Several clusters of self-associated species are present, exhibiting different salt dependencies and variable modulation by a surface charge mutation (Ser46 to Asp within a positively charged surface patch). Further, self-association can be completely eliminated upon addition of EIN to form the specific EIN–HPr complex. The distribution of the self-associated species was obtained using a similar approach to that employed to visualize the non-specific EIN–HPr encounter complexes.[17] The intermolecular PRE profiles originating from E5C and E32C were fit simultaneously by rigid body simulated annealing refinement using an ensemble of states to represent the distribution of one HPr molecule relative to another.[19] The analysis indicates that an optimal ensemble size of 4 with a population of ~1% is required to represent the self-associated state (Fig. 6b and c). Under the experimental conditions employed, this corresponds to a $K_{diss} \geq 15$ mM.[19]

While ultra-weak self-association of HPr is unlikely to be of any biological significance, it does demonstrate that PRE measurements can be used to detect and visualize transient, ultra-weak self-associated states of a protein in solution that are invisible to other biophysical techniques. The weak intermolecular interactions observed for HPr self-association encompass an ensemble of states and are driven by both electrostatic and hydrophobic interactions (Fig. 6c). This demonstration of principle paves the way to using intermolecular PRE measurements to characterize early stages of biologically significant oligomerization events, including the assembly of viral capsids[86] and the formation of amyloid fibrils.[87]

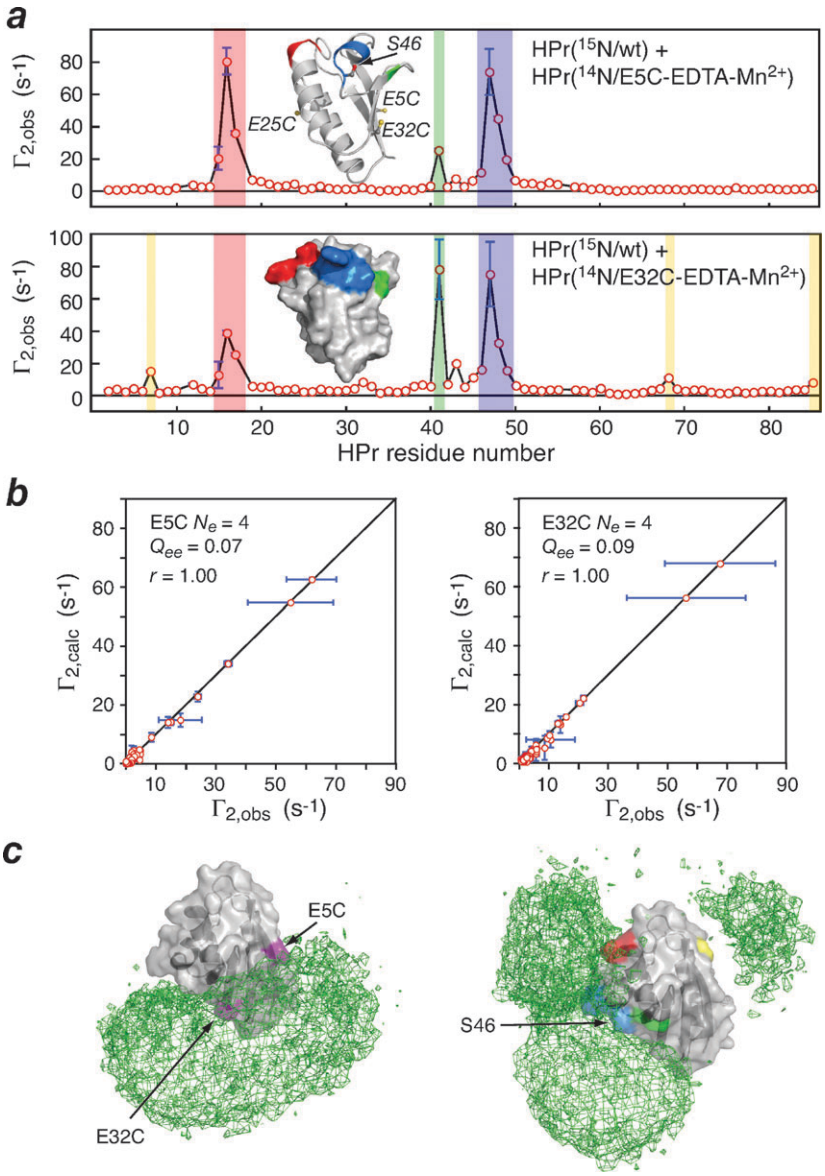

Fig. 6 Ultra-weak self-association of HPr. (a) Intermolecular PRE profiles and (b) correlation between observed and calculated (using an $N_e = 4$ ensemble representation) Γ_2 rates observed between ^{15}N-labeled wild type HPr and HPr conjugated to EDTA–Mn^{2+} at positions E5C and E32C. (c) Reweighted atomic probability density maps (green mesh), plotted at 20% threshold, showing the distribution of ^{15}N-labeled HPr relative to paramagnetically-labeled HPr (*left panel*, grey transparent surface and ribbon with the location of E5C and E32C indicated in magenta) and paramagnetically-labeled HPr relative to ^{15}N-labeled HPr (*right panel*, grey transparent surface and ribbon with the four groups of residues that experience large intermolecular PREs colored in red, green, blue and yellow using the same color scheme as in (a). Adapted from ref. 19.

Transient, lowly-populated states sampled by large-scale domain motions

Large-scale domain rearrangements in proteins often play a critical function in ligand binding, recognition, catalysis and regulation.[88–94] Crystal and NMR structures have provided a static picture of the *apo* (usually open) and *holo* (usually closed) states, but the general question remains as to whether the *apo* state exists as a single species in which the *holo* conformation (in the absence of ligand) is energetically inaccessible and interdomain rearrangement is induced by ligand binding, or whether the predominantly *apo* conformation coexists in rapid equilibrium with an alternative, lowly-populated, excited species which may correspond to a greater or lesser degree to the *holo* conformation. The PRE provides a powerful method to examine such phenomena.[18]

Maltose binding protein (MBP) is a classic example of a protein undergoing large interdomain rearrangement which has been extensively studied by crystallography,[93,94] NMR spectroscopy[95–97] and other biophysical techniques.[97–99] Upon sugar binding a $\sim 35^\circ$ rigid body domain reorientation between the N- (NTD) and C- (CTD) terminal domains occurs, involving hinge-bending within the linker region connecting the two domains.[93,94] RDCs measured on the *apo* and *holo* states are fully consistent with the respective crystal structures.[96] This is hardly surprising because the RDC observable is a linear weighted average of the species present in solution and is therefore insensitive to lowly-populated states.[18,100]

MBP was paramagnetically labeled with a nitroxide spin-label conjugated to surface engineered cysteine residues, D41C and S211C (one at a time), located in the NTD and CTD, respectively.[18] The PRE data for the sugar-bound *holo* form are entirely consistent with the crystal structure of *holo* MBP (PRE *Q*-factor of 0.18). In the case of *apo* MBP, however, the intradomain PRE data are in agreement with the structure, but the interdomain PRE data arising from the nitroxide at D41C exhibit regions with large discrepancies between observed and calculated PRE values (with an interdomain PRE *Q*-factor of 0.49) (Fig. 7a and b, left panel). These discrepancies cannot be accounted for by the presence of a small amount of *holo* conformation in rapid equilibrium with the *apo* conformation since a linear combination of these two states results in a minimal decrease in the PRE *Q*-factor for the D41C data and an increase in the PRE *Q*-factor for the S211C data. This finding is fully consistent with an extrapolated population of $\sim 0.002\%$ for the *holo* conformation derived from thermodynamic data.[97] Although the PRE data for *apo* MBP can be accounted for by a single alternative domain orientation of the NTD and CTD that is different from that in both the *apo* and *holo* structures, this alternative structure is inconsistent with the RDC data.[18] Thus, *apo* MBP must exist as a rapidly exchanging mixture comprising the predominant *apo* (open) state and a minor species. The

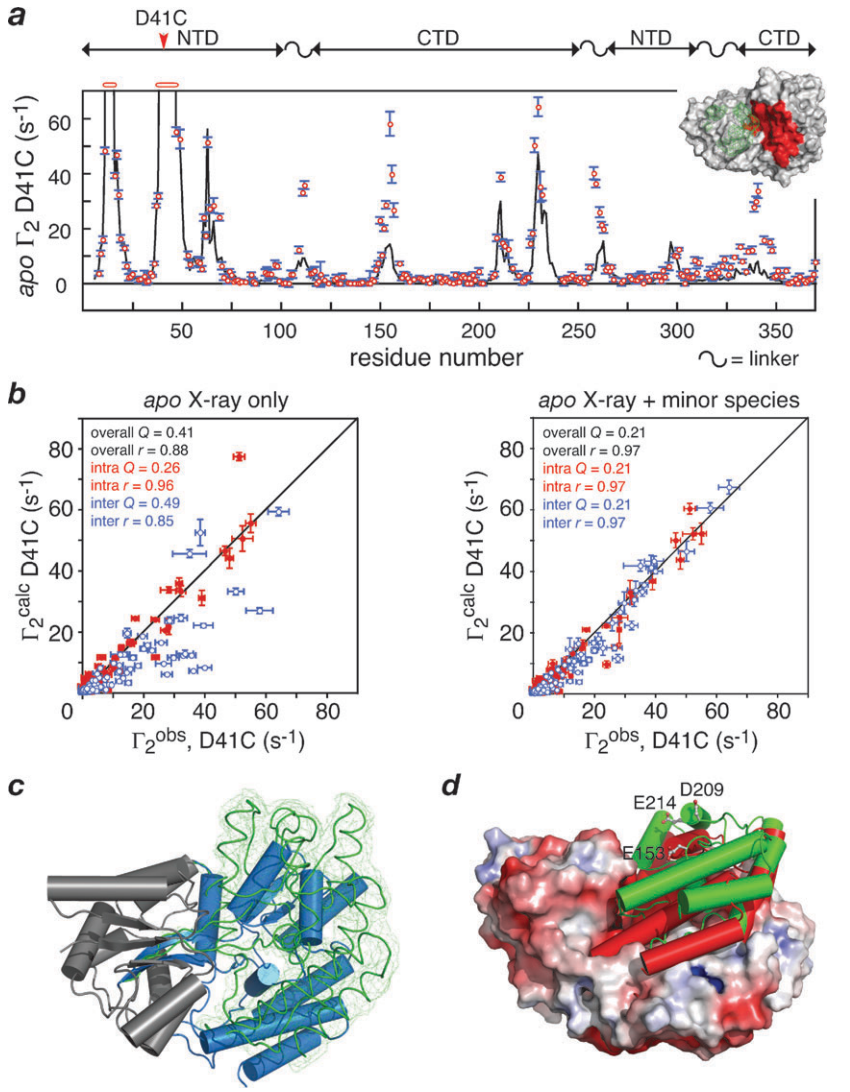

Fig. 7 Open-to-partially closed transition in *apo* MBP. (a) Comparison of observed PRE profiles (red circles) with back-calculated values obtained by ensemble paramagnetic probe refinement against the intermolecular PRE data for the nitroxide spin-label at D41C. (b) Comparison of observed *versus* calculated Γ_2 rates for the D41C data obtained with the X-ray *apo* MBP structure alone (*left panel*) and upon inclusion of a minor species at an occupancy of 5% (*right panel*). (c) Equilibrium mixture of the major open (blue cylinder) and minor partially-closed (green smoothed backbone trace with reweighted backbone atomic probability map shown as a green mesh) forms of the CTD of *apo* MBP with the NTDs of the two species superimposed and colored in grey. (d) Structural comparison of the CTD of the minor partially-closed state of *apo* MBP (green cylinders) and *holo* MBP (red cylinders) with the open form of *apo* MBP shown as a molecular surface color-coded according to electrostatic potential. Adapted from ref. 18.

time scale for interconversion between the two states has an upper limit of ~20 μs from relaxation dispersion experiments and a lower limit of ~20 ns (corresponding to the rotational correlation time of MBP) from $\{^{15}N\}$–^{1}H heteronuclear NOE data.[18]

The $\langle r^{-6}\rangle$ average structure of the minor species of *apo* MBP can be determined by conjoined rigid-body/torsion angle simulated annealing refinement[101,102] in which the PRE data originating from the D41C and S211C nitroxide labels are fitted simultaneously to a two-member ensemble of major open and minor species. The major species is held fixed in the *apo* crystal structure conformation whereas the domains of the minor species are allowed to move as rigid bodies by giving the linker residues torsional degrees of freedom. These calculations fully account for all the *apo* MBP PRE data with PRE *Q*-factors of 0.21 and 0.24 for the PREs originating from the D41C and S211C nitroxide labels (Fig. 7b, right panel), respectively, and, combined with RDC data, indicate that the population of the minor species is 5–7%.[18]

The minor species of *apo* MBP represents a partially closed state (Fig. 7c).[18] The transition between major (open) and minor (partially closed) forms of *apo* MBP involves a hinge rotation of ~33°, comparable to the 35° rotation between open *apo* and closed *holo* MBP. However, the *apo* minor and closed *holo* states are not the same and are related by a domain reorientation of ~18° accompanied by a ~6 Å translation (Fig. 7d). The interface between the NTD and CTD domains is lined by negatively charged residues that are responsible for an array of hydrogen bonds with the sugar substrate in *holo* MBP.[83,84] When the substrate is removed, the energy landscape is altered and access to the *holo* structure is energetically highly unfavorable as a result of electrostatic repulsion and lack of interdomain surface complementarity within the ligand-binding pocket that cannot be offset by bridging water molecules. These unfavorable interdomain interactions are circumvented in the partially closed *apo* state by translation of the CTD out of the sugar-binding pocket, thereby exposing several negatively charged residues, and, in addition, leaving the sugar binding surface on the CTD exposed.[18]

The PRE results for *apo* MBP prove the existence of dynamic equilibrium between a predominant (~95%) open state and a minor (~5%) partially-closed state. The presence of the minor species in *apo* MBP may facilitate the transition to the *holo* conformation that is only rendered energetically accessible by intermolecular interactions between the two domains and the sugar ligand. Thus the predominant fluctuations in *apo* MBP do not involve the energetically disfavored *holo* conformation and therefore the conformational change upon ligand binding can be viewed as an example of induced fit.[18]

Concluding remarks

The PRE provides a powerful tool for studying both structure and large-scale

dynamic phenomena involving macromolecules and their complexes in solution.

The application of the PRE for structure determination of complexes or multidomain proteins is restricted to systems in slow exchange. In fast exchanging systems, the PRE provides a direct means of detecting, characterizing and visualizing low population transient species. Thus the PRE provides a means to explore regions of the free energy landscape of biological macromolecular systems that are inaccessible to conventional structural and biophysical techniques, thereby opening a whole new field of study for structural biology.

Acknowledgements

This work was supported by the Intramural Program of the National Institute of Diabetes and Digestive and Kidney Diseases, National Institutes of Health. I thank Attila Szabo for useful discussions.

References

1 O. Miyashita, J. N. Onuchic and P. G. Wolynes, *Proc. Natl. Acad. Sci. U. S. A.*, 2003, **100**, 12570–12574.
2 O. G. Berg and P. H. von Hippel, *Annu. Rev. Biophys. Biophys. Chem.*, 1985, **14**, 1310160.
3 H. X. Zhou and A. Szabo, *Phys. Rev. Lett.*, 2004, **93**, 178101.
4 P. H. von Hippel and O. G. Berg, *J. Biol. Chem.*, 1989, **264**, 675–678.
5 S. E. Halford and J. F. Marko, *Nucleic Acids Res.*, 2004, **32**, 3040–3052.
6 G. Schreiber and A. R. Fersht, *Nat. Struct. Biol.*, 1996, **3**, 427–431.
7 M. Vijayakumar, K. Y. Wong, G. Schrieber, A. R. Fersht, A. Szabo and H. X. Zhou, *J. Mol. Biol.*, 1998, **278**, 1015–1024.
8 T. Selzer, S. Albeck and G. Schreiber, *Nat. Struct. Biol.*, 2000, **7**, 537–541.
9 S. H. Northrup, J. O. Boles and J. C. L. Reynolds, *Science*, 1988, **241**, 67–70.
10 R. R. Gabdouilline and R. C. Wade, *Curr. Opin. Struct. Biol.*, 2002, **12**, 204–213.
11 A. Spaar, C. Dammer, R. R. Gabdoulline, R. C. Wade and V. Helms, *Biophys. J.*, 2006, **90**, 1913–1924.
12 A. G. Palmer, M. J. Grey and C. Wang, *Methods Enzymol.*, 2005, **394**, 430–465.
13 A. G. Palmer and F. Massi, *Chem. Rev.*, 2006, **106**, 1700–1719.
14 J. P. Loria, R. B. Berlow and E. D. Watt, *Acc. Chem. Res.*, 2008, **41**, 214–221.
15 D. M. Korzhnev and L. E. Kay, *Acc. Chem. Res.*, 2008, **41**, 442–451.
16 J. Iwahara and G. M. Clore, *Nature*, 2006, **440**, 1227–1230.
17 C. Tang, J. Iwahara and G. M. Clore, *Nature*, 2006, **444**, 383–386.
18 C. Tang, C. D. Schwieters and G. M. Clore, *Nature*, 2007, **449**, 1078–1082.
19 C. Tang, R. Ghirlando and G. M. Clore, *J. Am. Chem. Soc.*, 2008, **130**, 4048–4056.
20 A. N. Volkov, J. A. R. Worall, H. Holtzmann and M. Ubbink, *Proc. Natl. Acad. Sci. U. S. A.*, 2006, **103**, 18945–18950.
21 G. M. Clore, C. Tang and J. Iwahara, *Curr. Opin. Struct. Biol.*, 2007, **17**, 603–616.
22 I. N. Serdyuk, N. R. Zaccai and J. Zaccai, *Methods in Molecular Biophysics Structure Dynamics and Function*, Cambridge University Press, Cambridge, 2007.
23 P. Vallurupalli, D. F. Flemming, E. Stollar, E. Meirovitch and L. E. Kay, *Proc. Natl. Acad. Sci. U. S. A.*, 2007, **104**, 18473–18477.
24 P. Vallurupalli, D. F. Hansen and L. E. Kay, *J. Am. Chem. Soc.*, 2008, **130**, 2734–2735.
25 D. F. Hansen, P. Vallurupalli and L. E. Kay, *J. Am. Chem. Soc.*, 2008, **130**, 8397–8405.
26 D. M. Korzhnev, X. Salvatella, M. Vendruscolo, A. A. Di Nardo, A. R. Davidson, C. M. Dobson and L. E. Kay, *Nature*, 2004, **430**, 586–590.
27 K. Sugase, H. J. Dyson and P. E. Wright, *Nature*, 2007, **447**, 1021–1025.
28 D. D. Boehr, D. McElheny, H. J. Dyson and P. E. Wright, *Science*, 2006, **313**, 1638–1642.
29 M. J. Grey, C. Y. Wang and A. G. Palmer, *J. Am. Chem. Soc.*, 2003, **125**, 14324–14335.
30 D. Tolkatchev, P. Xu and F. Ni, *J. Am. Chem. Soc.*, 2003, **125**, 12432–12442.
31 I. Solomon, *Phys. Rev.*, 1955, **99**, 559–565.
32 N. Bloembergen and L. O. Morgan, *J. Chem. Phys.*, 1961, **34**, 842–850.
33 K. Wüthrich, *NMR of Proteins and Nucleic Acids*, John Wiley, New York, 1986.
34 G. M. Clore and A. M. Gronenborn, *Annu. Rev. Biophys. Biophys. Chem.*, 1991, **20**, 29–63.
35 H. Cheng and J. L. Markley, *Annu. Rev. Biophys. Biomol. Struct.*, 1995, **24**, 209–237.
36 I. Bertini, C. Luchinat and M. Licciolini, *Methods Enzymol.*, 2001, **339**, 314–340.
37 M. Ubbink, J. A. R. Worral, G. W. Canters, E. J. J. Groenen and M. Huber, *Annu. Rev. Biophys. Biomol. Struct.*, 2002, **31**, 393–422.
38 P. A. Kosen, *Methods Enzymol.*, 1989, **177**, 86–121.
39 P. G. Schmidt and I. D. Kuntz, *Biochemistry*, 1984, **23**, 4261–4266.
40 P. A. Kosen, R. M. Scheek, H. Naderi, V. J. Basus, S. Manogaran, P. G. Schmidt, N. J. Oppenheimer and I. D. Kuntz, *Biochemistry*, 1986, **25**, 2356–2364.
41 J. R. Gillespie and D. Shortle, *J. Mol. Biol.*, 1997, **268**, 158–169.
42 J. L. Battiste and G. Wagner, *Biochemistry*, 2000, **39**, 5355–5365.
43 V. Gaponenko, J. W. Howarth, G. Columbus, J. Gasmi-Seabrook, W. L. Yuan, P. R. Hubbel and P. R. Rosevear, *Protein Sci.*, 2000, **9**, 302–309.
44 L. W. Donaldson, W. Y. Skrynnikov, D. R. Choy, B. Muhandiram, J. D. Sarkar, J. D. Forman-Kay and L. E. Kay, *J. Am. Chem. Soc.*, 2001, **123**, 9843–9847.
45 A. Dvortezky, V. Gaponenko and P. R. Rosevear, *FEBS Lett.*, 2002, **528**, 189–192.
46 G. Pintacuda, A. Mosref, A. Leonchiks, A. Shapiro and G. Otting, *J. Biomol. NMR*, 2004, **29**, 351–361.
47 T. K. Mal, M. Ikura and L. E. Kay, *J. Am. Chem. Soc.*, 2002, **124**, 14002–14003.
48 J. D. Gross, N. J. Moerke, R. von der Haar, A. A. Lugovsky, A. B. Sachs, J. E. McCarthy and G. Wagner, *Cell (Cambridge, MA, US)*, 2003, **115**, 739–750.
49 P. B. Card, P. J. A. Erbel and K. H. Gardner, *J. Mol. Biol.*, 2005, **353**, 664–677.
50 P. E. Johnson, E. Brun, F. MacKenzie, S. G. Withers and L. P. McIntosh, *J. Mol. Biol.*, 1999, **287**, 609–625.
51 C. W. Bertoncini, Y. S. Jung, C. O. Fernandez, W. Hoyer, C. Griesinger, T. M. Jovin and M. Zweckstetter, *Proc. Natl. Acad. Sci. U. S. A.*, 2005, **102**, 1430–1435.
52 M. M. Dedmon, K. Lindorff-Larsen, J. Christodoulou, M. Vendruscolo and C. M. Dobson, *J. Am. Chem. Soc.*, 2005, **127**, 476–477.
53 A. Ramos and G. Varani, *J. Am. Chem. Soc.*, 1998, **120**, 10992–10993.
54 J. Iwahara, D. E. Anderson, E. C. Murphy and G. M. Clore, *J. Am. Chem. Soc.*, 2003, **125**, 6634–6635.
55 J. Iwahara, C. D. Schwieters and G. M. Clore, *J. Am. Chem. Soc.*, 2004, **126**, 12800–12808.
56 J. Iwahara, C. D. Schwieters and G. M. Clore, *J. Am. Chem. Soc.*, 2003, **125**, 6634–6635.
57 A. Hillisch, M. Lorenz and S. Diekmann, *Curr. Opin. Struct. Biol.*, 2001, **11**, 201–207.
58 G. E. Fanucci and D. S. Cafiso, *Curr. Opin. Struct. Biol.*, 2006, **16**, 644–653.
59 C. S. Klug and J. B. Feix, *Methods Cell Biol.*, 2008, **84**, 617–657.
60 L. Galiano, M. Bonora and G. E. Fanucci, *J. Am. Chem. Soc.*, 2007, **129**, 11004–11005.
61 C. Altenbach, A. K. Kuznetzow, O. P. Ernst, K. P. Hofmann and W. L. Hubbell, *Proc. Natl. Acad. Sci. U. S. A.*, 2008, **105**, 7439–7444.
62 J. Iwahara, C. Tang and G. M. Clore, *J. Magn. Reson.*, 2007, **184**, 185–195.
63 W. J. Gehring, Y. Q. Qian, M. Billeter, K. Furukubo-Tokunaga, A. F. Schier, D. Resendez-Perez, M. Affolter, G. Otting and K. Wüthrich, *Cell (Cambridge, MA, US)*, 1994, **78**, 211–223.
64 E. Fraenkel and C. O. Pabo, *Nat. Struct. Biol.*, 1998, **5**, 692–697.
65 M. Billeter, Y. Q. Qian, G. Otting, M. Müller, W. J. Gehring and K. Wüthrich, *J. Mol. Biol.*, 1993, **234**, 1084–1093.
66 M. Affolter, A. Percival-Smith, M. Müller, W. Leupin and W. J. Gehring, *Proc. Natl. Acad. Sci. U. S. A.*, 1990, **87**, 4093–4097.
67 K. M. Caltron, N. Iler and C. Abate, *Mol. Cell. Biol.*, 1993, **13**, 2354–2365.

68 J. Iwahara and G. M. Clore, *J. Am. Chem. Soc.*, 2006, **128**, 404–405.
69 T. Misteli, *Science*, 2001, **291**, 843–847.
70 J. Iwahara, M. Zweckstetter and G. M. Clore, *Proc. Natl. Acad. Sci. U. S. A.*, 2006, **103**, 15062–15067.
71 D. S. Garrett, Y. J. Seok, A. Peterkofsky, A. M. Gronenborn and G. M. Clore, *Nat. Struct. Biol.*, 1999, **6**, 166–173.
72 D. S. Garrett, Y. J. Seok, A. Peterkofksy, G. M. Clore and A. M. Gronenborn, *Biochemistry*, 1997, **36**, 4393–4398.
73 D. I. Liao, E. Silverton, Y. J. Seok, B. R. lee, A. Peterkofsky and D. R. Davies, *Structure*, 2006, **4**, 861–872.
74 Z. Jia, J. W. Quail, E. B. Waygood and L. T. Delbaere, *J. Biol. Chem.*, 1993, **268**, 22490–22501.
75 D. S. Garrett, Y. J. Seok, D. I. Liao, A. Peterkofksy, A. M. Gronenborn and G. M. Clore, *Biochemistry*, 1997, **36**, 2517–2530.
76 N. A. van Nuland, I. W. Hangvi, R. C. van Schaik, H. J. Berendsen, W. F. van Gunsteren, R. M. Scheek and G. T. Robbilard, *J. Mol. Biol.*, 1994, **237**, 544–559.
77 M. Wittekind, P. Rajgopal, B. R. Branchini, J. Reizer, M. H. Saier and R. E. Klevit, *Protein Sci.*, 1992, **1**, 1363–1376.
78 C. D. Schwieters, J. Kuszewski and G. M. Clore, *Prog. Nucl. Magn. Reson. Spectrosc.*, 2006, **48**, 47–62.
79 C. D. Schwieters and G. M. Clore, *J. Biomol. NMR*, 2002, **23**, 221–225.
80 J.-Y. Suh, C. Tang and G. M. Clore, *J. Am. Chem. Soc.*, 2007, **129**, 12954–12955.
81 Y. Levy, P. G. Wolynes and J. N. Onuchic, *Proc. Natl. Acad. Sci. U. S. A.*, 2004, **101**, 511–516.
82 R. Alsallaq and H. X. Zhou, *Biophys. J.*, 2007, **92**, 1486–1502.
83 Y. C. Kim, C. Tang, G. M. Clore and G. Hummer, *Proc. Natl. Acad. Sci. U. S. A.*, 2008, **105**, 12855–12860.
84 X. Xu, W. Reinle, F. Hannemann, P. V. Konarev, D. I. Svergun, R. Bernhardt and M. Ubbink, *J. Am. Chem. Soc.*, 2008, **130**, 6395–6403.
85 J. M. Garcia-Ruiz, *J. Struct. Biol.*, 2003, **142**, 22–31.
86 A. Zlotnick, *J. Mol. Recognit.*, 2005, **18**, 470–490.
87 N. L. Fawzi, Y. Okabe, E. H. Yap and T. Head-Gordon, *J. Mol. Biol.*, 2007, **365**, 535–550.
88 C. M. Anderson, F. H. Zucker and T. A. Steitz, *Science*, 1979, **204**, 375–380.
89 M. Gerstein, A. M. Lesk and C. Chothia, *Biochemistry*, 1994, **33**, 6739–6749.
90 S. Hayward and H. J. Berendsen, *Proteins: Struct., Funct., Genet.*, 1998, **30**, 144–154.
91 M. Wolf-Watz, V. Thai, K. Henzler-Wildman, G. Hadjipavlou, E. Z. Eisenmesser and D. Kern, *Nat. Struct. Biol.*, 2004, **11**, 945–949.
92 K. A. Henzler-Wildman, V. Thai, M. Lei, M. Ott, M. Wolf-Watz, T. Fenn, E. Pozharski, M. A. Wilson, G. A. Petsko, M. Karplus, C. G. Hübner and D. Kern, *Nature*, 2007, **450**, 838–844.
93 A. J. Sharff, L. E. Rodseth, J. C. Spurlino and F. A. Quiocho, *Biochemistry*, 1992, **31**, 10657–10663.
94 F. A. Quiocho, J. C. Spurlino and L. E. Rodseth, *Structure*, 1997, **5**, 997–1015.
95 N. R. Skrynnikov, N. K. Goto, D. Yang, W. Y. Choy, J. R. Tolman, G. A. Mueller and L. E. Kay, *J. Mol. Biol.*, 2000, **295**, 1265–1273.
96 J. Eneväs, V. Tugarinov, N. R. Skynnikov, N. K. Goto, R. Muhandiram and L. E. Kay, *J. Mol. Biol.*, 2001, **309**, 961–974.
97 O. Millet, R. P. Hudson and L. E. Kay, *Proc. Natl. Acad. Sci. U. S. A.*, 2003, **100**, 12700–12705.
98 J. A. Hall, T. E. Thorgeirsson, J. Liu, Y. K. Shin and H. Nikaido, *J. Biol. Chem.*, 1997, **272**, 17615–17622.
99 Y. Zhang, P. J. Gardina, A. S. Kuebler, H. S. Kang, J. A. Christopher and M. D. Manson, *Proc. Natl. Acad. Sci. U. S. A.*, 1999, **96**, 939–944.
100 A. Bax, *Protein Sci.*, 2003, **12**, 1–16.
101 G. M. Clore and C. A. Bewley, *J. Magn. Reson.*, 2002, **154**, 329–335.
102 C. D. Schwieters and G. M. Clore, *J. Magn. Reson.*, 2001, **152**, 288–302.